

3D Robust Adaptive Region Growing for segmenting [18F]fluoride ion PET images

T. Grenier, *Associate Member, IEEE*, C. Revol-Muller, N. Costes, M. Janier and G. Gimenez

Abstract - We propose a new **Robust Adaptive Region Growing method (RoAd RG)** based on two local parameters: the local mean value of the intensity function and the local mean value of the norm of the intensity gradient. This approach enables a better spread of the region growing inside the region of interest while avoiding the merge of outlier pixels. We tested our method on a synthesized noisy image, and demonstrated that RoAd RG gives better result than non adaptive or not fully adaptive methods. We applied positively our method to 3D [18F]fluoride ion PET images for segmenting bone structures, and showed its superiority compared to a non adaptive method.

I. INTRODUCTION

SEGMENTATION is an important step in medical imaging for feature extraction and quantitative analysis of images. Concretely, this process aims at delineating automatically anatomical structures. A lot of techniques for image segmentation are available today. Many methods were proposed (see surveys [1-4]) and some works tried to unify different segmentation approaches [5, 6].

Apart from contour based approaches, region based methods, especially region growing approaches, are often used in software for semi-manual image segmentation. Initially introduced by Zucker [7], region growing is based on a similarity measure between neighboring pixels and region of interest. This approach is quite attractive for its simplicity (easy to initialize, to tune and to stop) and for its speed. The algorithm of region growing can be summarily described as an iterative procedure based on two steps: i)

find all neighboring pixels of a previous segmented region $R^{[l]}$, not belonging yet to $R^{[l]}$ (for simplicity, we call them *eligible* pixels), ii) among these pixels, select those satisfying a homogeneity criterion and merge them to $R^{[l]}$. Then, the new region, noted $R^{[l+1]}$, replaces $R^{[l]}$.

Let us notice that $R^{[0]}$ must be initialized by some special pixels called initial seeds included in the object to segment. For lots of region growing methods, the final segmentation depends on the choice of these initial seeds. The homogeneity criterion governing the merge of the pixels is usually based on a similarity measure between the intensities of the eligible pixels and the intensities of the pixels belonging to the growing region (mean value [8, 9] or other statistical parameters [10, 11] are classically used).

In this framework, we focus on the segmentation of [18F]fluoride ion PET images. The radioactive substance [18F]fluoride ion (NaF) is the standard agent and an excellent indicator of bones metabolism [12]. In [18F]fluoride ion PET studies, high variations of the tracer uptake inside the bone structures combined with the low resolution of images make the segmentation task very arduous and require the development of adaptive approaches. Some adaptive region growing methods [10, 13, 14] were proposed in the literature but not applied to PET images. To tackle this problem, we have developed a 3D **Robust Adaptive Region Growing** method called **RoAd RG**, based on the local mean values of the gray levels and also the intensity gradient. This method is particularly well adapted to the segmentation of images characterized by high variations of intensity.

In section 2, we describe **RoAd RG** and its adaptive parameters. In the third section, we compare our method with two other methods, using a synthesized test image. In the fourth section, we examine and compare the efficiency of our method for segmenting bone structures in a real [18F]fluoride ion PET image.

II. PRINCIPLE OF ROAD RG

In this section, we present the principle of our **Robust Adaptive Region Growing** method **RoAd RG** and its main features.

Manuscript received November 28, 2003.

T. Grenier is with the REsearch and Applications Center for Image and Signal Processing (CREATIS), Blaise Pascal, 69621 Villeurbanne Cedex, FRANCE (e-mail: thomas.grenier@creatis.insa-lyon.fr).

C. Revol-Muller is with the CREATIS, Blaise Pascal, 69621 Villeurbanne Cedex, FRANCE (e-mail: muller@creatis.insa-lyon.fr).

N. Costes is with the Medical Exploration and Research Center for Positron Emission (CERMEP), 59 Bd Pinel, 69003 Lyon, FRANCE (e-mail: costes@cermep.fr).

M. Janier is with both the CREATIS and the CERMEP, FRANCE (e-mail: janier@univ-lyon1.fr).

G. Gimenez is with both the CREATIS and the CERMEP, FRANCE (e-mail: gerard.gimenez@creatis.insa-lyon.fr).

Research and Applications Center for Image and Signal Processing (CREATIS) is a C.N.R.S. research unit (UMR 5515) and a INSERM research unit (U630) common to the National Institute of Applied Sciences of Lyon (INSA Lyon) and to the University Claude Bernard-Lyon1.

A. Local parameters

Our method is based on two local measures:

- $\mu_x^{[t]}$ mean value of pixel intensities computed from a special neighborhood of pixel \mathbf{x} ,
- $\|\nabla\|_x^{[t]}$ mean value of the norm of the intensity gradient computed from another special neighborhood of \mathbf{x} .

Both measures depend on the pixel \mathbf{x} , the iteration t and two special neighborhoods defined below.

In classical methods, the mean value of the intensity is computed from the pixels of the whole growing region. In *RoAd RG*, the mean value is only computed from the pixels of the growing region which belongs to $\Omega_\mu^{[t]}(\mathbf{x})$ a neighborhood of \mathbf{x} included in this region. The neighborhood $\Omega_\mu^{[t]}(\mathbf{x})$ is shown in Fig. 1 and expressed in (1), where $d(\mathbf{x}, \mathbf{y})$ is the Euclidian distance between \mathbf{x} and \mathbf{y} and \mathcal{E} is a spatial radius.

$$\Omega_\mu^{[t]}(\mathbf{x}) = \{\mathbf{y} \in R^{[t]} \mid d(\mathbf{x}, \mathbf{y}) < \mathcal{E}\} \quad (1)$$

$\mu_x^{[t]}$ is computed from (2), where $\text{card}(A)$ is the number of pixels in a set A , and $I(\mathbf{y})$ represents the intensity of the pixel \mathbf{y} :

$$\mu_x^{[t]} = \frac{1}{\text{card}(\Omega_\mu^{[t]}(\mathbf{x}))} \sum_{\mathbf{y} \in \Omega_\mu^{[t]}(\mathbf{x})} I(\mathbf{y}) \quad (2)$$

The mean value of the norm of the intensity gradient is computed from all the pixels located in $\Omega_{\|\nabla\|}^{[t]}(\mathbf{x})$ a neighborhood of \mathbf{x} expressed in (3):

$$\Omega_{\|\nabla\|}^{[t]}(\mathbf{x}) = \{\mathbf{y} \in R^{[t]} \cup \overline{R^{[t]}} \mid d(\mathbf{x}, \mathbf{y}) < \xi\} \quad (3)$$

where ξ is a second spatial radius. $\|\nabla\|_x^{[t]}$ is computed from (4):

$$\|\nabla\|_x^{[t]} = \frac{1}{\text{card}(\Omega_{\|\nabla\|}^{[t]}(\mathbf{x}))} \sum_{\mathbf{y} \in \Omega_{\|\nabla\|}^{[t]}(\mathbf{x})} \|\nabla I(\mathbf{y})\| \quad (4)$$

Figure 1 illustrates the neighborhoods $\Omega_\mu^{[t]}(\mathbf{x})$ and $\Omega_{\|\nabla\|}^{[t]}(\mathbf{x})$ related to both local parameters.

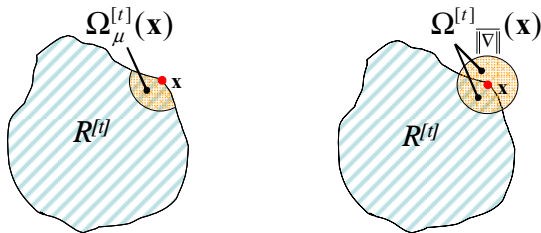


Fig. 1: Illustration of the two neighborhoods.

B. Homogeneity criterion

The choice of the homogeneity criterion is the most important point in the region growing methods. Equation (5) expresses the homogeneity criterion of *RoAd RG*, with $I(\mathbf{y})$

the intensity of the eligible pixel \mathbf{y} neighbor of \mathbf{x} , and $\mu_x^{[t]}, \|\nabla\|_x^{[t]}$ both previously defined local parameters.

$$\mu_x^{[t]} - \alpha \|\nabla\|_x^{[t]} < I(\mathbf{y}) < \mu_x^{[t]} + \beta \|\nabla\|_x^{[t]} \quad (5)$$

Although α and β are constant coefficients determining the allowed variation of intensities around the local mean value $\mu_x^{[t]}$, it must be noticed that our homogeneity criterion is fully adaptive: the tolerated variation is a function of the local gradient intensity $\|\nabla\|_x^{[t]}$. The pixels which intensity is outside this range of values are considered as outliers, i.e. as pixels not belonging to the homogeneous region.

C. RoAd RG algorithm

Repeat the following steps while $R^{[t+1]} \neq R^{[t]}$, i.e. until no more pixels can be added to $R^{[t]}$ the current growing region.

- 1- Clear the temporary set C ,
- 2- For each pixel $\mathbf{x} \in R^{[t]}$:

2.1- Determine the sets $\Omega_\mu^{[t]}(\mathbf{x})$ and $\Omega_{\|\nabla\|}^{[t]}(\mathbf{x})$ from (1)

and (3). Then, compute $\mu_x^{[t]}$ from (2) and $\|\nabla\|_x^{[t]}$ from (4),

2.2- Find $Y(\mathbf{x})$, the subset of eligible pixels located in a connected neighborhood of the pixel \mathbf{x} ,

2.3- Add to the temporary set C , each $\mathbf{y} \in Y(\mathbf{x})$ verifying the homogeneity criterion (5).

- 3- Assign $R^{[t+1]} = R^{[t]} \cup C$.

III. EXPERIMENTS

This section compares *RoAd RG* with two other region growing methods using a 2D synthesized test image.

A. Selected methods used for the comparison

We selected two region growing methods in order to evaluate the improvement of our fully adaptive approach compared to classical ones.

The first method is a non adaptive region growing algorithm. It is governed by a homogeneity criterion which depends on a global mean value of the intensities in $R^{[t]}$ and also on two constant thresholds (α and β) defining the bounds of the intensity variation around this global mean value. We called this method **Global Mean Region Growing** and we note it **GMRG**. The homogeneity criterion of **GMRG** is expressed by:

$$\mu^{[t]} - \alpha < I(\mathbf{y}) < \mu^{[t]} + \beta \quad (6)$$

The second method is a not fully adaptive region growing. It is governed by a homogeneity criterion defined in (7) which depends on a local mean value of the intensities (like *RoAd RG*) and two constant thresholds limiting the variation around this adaptive mean value. We note this method **AMRG**, for **Adaptive Mean Region Growing**.

$$\mu_x^{[t]} - \alpha < I(\mathbf{y}) < \mu_x^{[t]} + \beta \quad (7)$$

B. Synthesized data

We tested the three region growing methods (*GMRG*, *AMRG* and *RoAd RG*) on a 2D synthesized test image mimicking characteristics of [¹⁸F]fluoride ion PET images. The size of this image is 128x128 pixels coded by 8 bits. The artificial image represents a rectangular object placed in an inhomogeneous background. The intensities of the pixels in the object decrease vertically and horizontally as shown in Fig. 2a. A Gaussian noise ($\sigma = 25$) was added, resulting in the 2D test image presented in Fig. 2b

As *RoAd RG* is based on the norm of the intensity gradient, we display the result of a Prewitt filter applied to the test image in Fig. 2c.

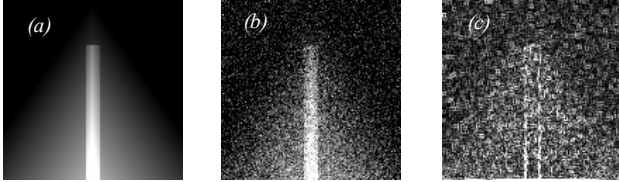


Fig. 2: (a) artificial image, (b) test image, (c) Prewitt filter.

In the next figure, we plot two profiles of intensity along the arrows drawn in the test image.

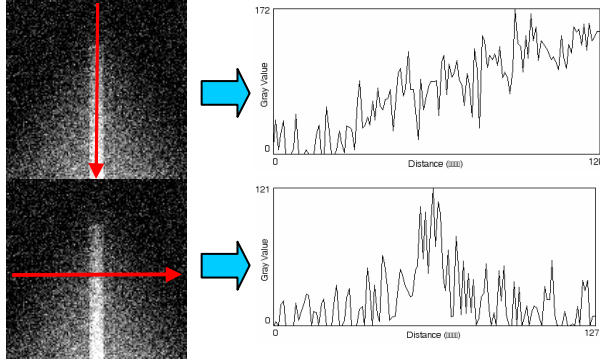


Fig. 3: Two profiles of intensity in the test image.

C. Results and discussion

The behavior of three methods was examined, by using two sets of initial seeds displayed in Fig. 4.

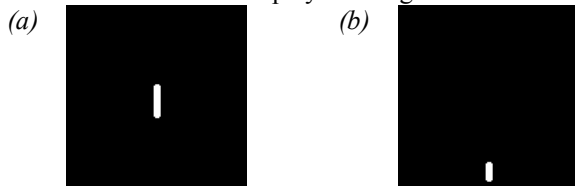


Fig. 4: Two initial sets of seeds for region growing: (a) middle set and (b) bottom set.

Figure 5 shows the results of the *GMRG*, *AMRG* and *RoAd RG* segmentations, initialized by the middle set (Fig. 4a). The parameters of the methods are specified below each image. In every case, α and β were manually tuned in

order to get the best results. It should be noted that $\beta > \alpha$ since the region of interest corresponds to pixels of high intensities. For *RoAd RG*, the spatial radii ε and ξ of the special neighborhoods used for the computation of the adaptive parameters $\mu_x^{[t]}$ and $\|\nabla\|_x^{[t]}$, were chosen equal to 4. For *AMRG*, ε was also equal to 4.

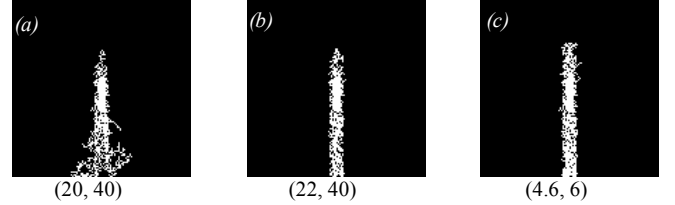


Fig. 5: Results of the three region growing methods initialized by the middle set: (a) *GMRG*, (b) *AMRG* and (c) *RoAd RG*.

The results of the three region growing methods initialized by the bottom set (Fig. 4b) are given in Fig. 6. The parameters were fixed to the same values as before.

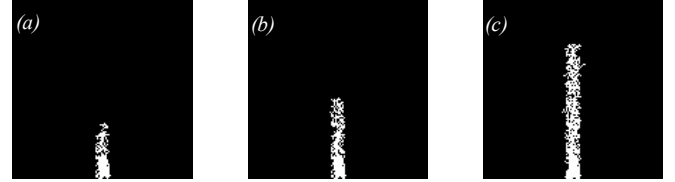


Fig. 6: Results of the three region growing methods initialized by the bottom set: (a) *GMRG*, (b) *AMRG* and (c) *RoAd RG*.

Fig. 5c and Fig. 6c show that in both cases, *RoAd RG* performs better than *GMRG* and *AMRG* methods. *RoAd RG* succeeds in segmenting the whole object despite inhomogeneity of intensity and noise. One advantage of our method is to be less dependent on the choice of the initial seeds.

IV. APPLICATION TO [¹⁸F]FLUORIDE ION IMAGES

In this section, we present briefly the 3D [¹⁸F]fluoride ion PET images and the results of *GMRG* and *RoAd RG* segmentations obtained from these data.

A. [¹⁸F]fluoride ion PET images

We use a standard protocol of [¹⁸F]fluoride ion PET described in [12] and used in a previous work [15]. A whole body NaF PET study is presented in Fig. 7a. The dimensions of the volume are 128x128x349 pixels and the gray levels are coded in short (2^{16}) format. The intensity values are proportional to the tracer uptake.

Two profiles of intensity are plotted in Fig. 7d and Fig. 7e. Both were extracted from the same slice located in the skull (Fig. 7b and Fig. 7c). The high variations of the intensity and the inhomogeneity of the uptake due to bone metabolism are underlined by the profiles. It should be noticed that these profiles fairly appear like those obtained from the test image (Fig. 3).

B. Results and discussion

We focus on the segmentation of the skull and the spinal column in whole body [^{18}F]fluoride ion PET studies. We compare our method (*RoAd RG*) with the non-adaptive region growing method (*GMRG*). In both methods, the initial seeds are automatically located by a procedure we presented in [15].

The settings of *RoAd RG* are $\alpha = 0.8$; $\beta = 5$; $\varepsilon = \xi = 3$. The settings of *GMRG* are $\alpha = 900$; $\beta = 18000$. These parameters were manually adjusted in order to get results as good as possible.

Figure 8c and Fig. 8d display the results of the segmentation with *GMRG* and *RoAd RG*. In the skull, *RoAd RG* leads to a better segmentation than *GMRG*, since the segmented region has successfully spread over the whole structure despite the high variations of the intensities. That demonstrates the improvements provided by the use of the adaptive parameters. It can be noticed that some parts of the skull still remain not segmented: this phenomenon can be explained by a very high local variation of the intensity due to a lack of the tracer uptake.

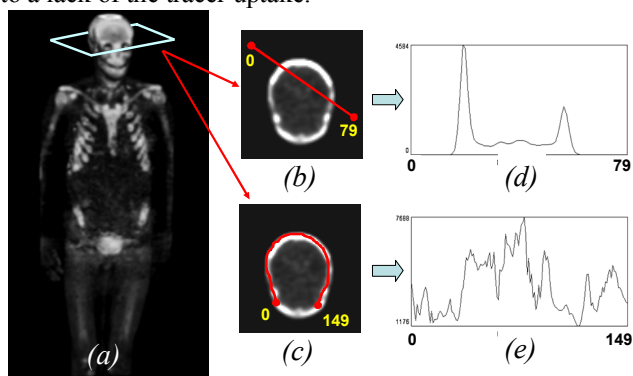


Fig. 7: (a) Whole body [^{18}F]fluoride ion PET image; (b), (c) the same slices in the skull; (d), (e) two profiles of intensity.

V. CONCLUSION

We have proposed a new Robust Adaptive Region Growing method (*RoAd RG*) based on two local parameters: the local mean value of the intensity function and the local mean value of the norm of the intensity gradient. We have tested our method on a synthesized noisy image and shown that *RoAd RG* gives better results than non adaptive or not fully adaptive methods, since it enables a better spread of the segmentation while avoiding the merge of outlier pixels. We have also applied positively our method to [^{18}F]fluoride ion PET images. In a future work, we will assess quantitatively our method using 3D synthesized images and simulated PET data.

VI. REFERENCES

- [1] K. S. Fu and J. K. Mui, "A survey on image segmentation," *Pattern Recognition*, vol. 13, pp. 3-16, 1981.
- [2] R. M. Haralick and L. G. Shapiro, "Survey: Image segmentation techniques," *Comput. Vision Graphics Image Process.*, vol. 29, pp. 100-132, 1985.
- [3] N. R. Pal and S. K. Pal, "A review on image segmentation techniques," *Pattern Recognition*, vol. 26, pp. 1277-1294, 1993.
- [4] A. K. Jain, M. N. Murty, and P. J. Flynn, "Data clustering: a review," *ACM Comput. Surv.*, vol. 31, pp. 264-323, 1999.
- [5] S. C. Zhu and A. Yuille, "Region competition: unifying snakes, region growing, and Bayes/MDL for multiband image segmentation," *IEEE Transactions on Pattern Analysis and Machine Intelligence*, vol. 18, pp. 884-900, 1996.
- [6] T. Zouagui, H. Benoit-Cattin, and C. Odet, "Image segmentation functional model," *Pattern Recognition*, vol. 37, pp. 1785-1795, 2004.
- [7] S. W. Zucker, "Region growing: childhood and adolescence," *Computer Graphics Image Processing*, vol. 5, pp. 382-399, 1976.
- [8] R. Adams and L. Bischof, "Seeded region growing," *IEEE Transactions on Pattern Analysis and Machine Intelligence*, vol. 16, pp. 641-647, 1994.
- [9] A. Mehnert and P. Jackway, "Improved seeded region growing algorithm," *Pattern Recognition Letters*, vol. 18, pp. 1065-1071, 1997.
- [10] R. Pohle and K. D. Toennies, "Segmentation of medical images using adaptive region growing," presented at Medical Imaging 2001 Image Processing, Feb 19-22 2001, San Diego, CA, 2001.
- [11] C. Revol-Muller, F. Peyrin, Y. Carrillon, and C. Odet, "Automated 3D region growing algorithm based on an assessment function," *Pattern Recognition Letters*, vol. 23, pp. 137-150, 2002.
- [12] C. K. Hoh, R. A. Hawkins, M. Dahlbom, J. A. Glaspy, L. L. Seeger, Y. Choi, C. W. Schiepers, S. C. Huang, N. Satyamurthy, J. R. Barrio, and et al., "Whole body skeletal imaging with [^{18}F]fluoride ion and PET," *J Comput Assist Tomogr*, vol. 17, pp. 34-41, 1993.
- [13] J. Yi and J. B. Ra, "A locally adaptive region growing algorithm for vascular segmentation," *International Journal of Imaging Systems and Technology*, vol. 13, pp. 208-214, 2003.
- [14] Y.-L. Chang and X. Li, "Adaptive image region-growing," *IEEE Transactions on Image Processing*, vol. 3, pp. 868-872, 1994.
- [15] T. Grenier, C. Revol-Muller, N. Costes, M. Janier, and G. Gimenez, "Automated seeds location for whole body NaF PET segmentation," *IEEE Trans. Nuc. Sci.*, vol. 52, pp. 1401-1405, 2005.

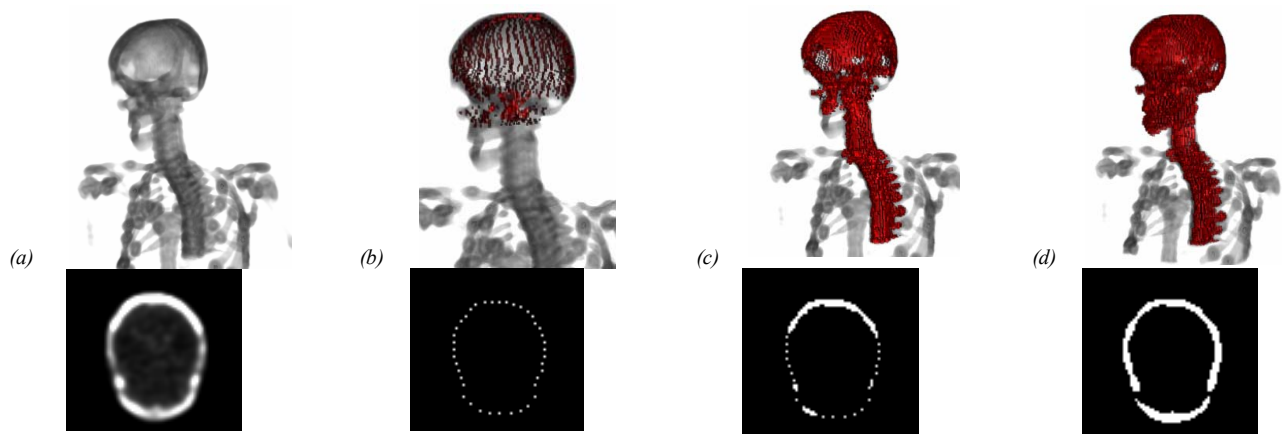


Fig. 8: Application on $[^{18}\text{F}]$ fluoride ion PET image: (a) original data, (b) initial seeds (obtained from [15]), (c) *GMRG* results, (d) *RoAdRG* results. For each column, 3D representation is given at the top and a slice located in the skull is given at the bottom.